Kinetics of carrier-induced degradation at elevated temperature in multicrystalline silicon solar cells

Wolfram Kwapil[a,b,*], Tim Niewelt[a,b], Martin C. Schubert[a]

[a] Fraunhofer Institute for Solar Energy Systems (ISE), Heidenhofstr. 2, 79110 Freiburg, Germany
[b] Freiburg Material Research Center (FMF), Stefan-Meier-Str. 21, 79100 Freiburg, Germany

A B S T R A C T

The degradation kinetics of multicrystalline silicon solar cells and wafers at elevated temperature (often termed "LeTID") depend on the specific temperature and injection conditions. We apply different forward biases in the dark at a constant temperature of ~75 °C to industrial passivated emitter rear contacted (PERC) solar cells fabricated on p-type multicrystalline wafers from a variety of material producers and determine the degradation rate constant in dependence of the excess carrier density at the p-n junction. We find that whereas the specific material properties influence the degradation extent, the degradation rate constant is comparable for all materials but depends on the excess carrier concentration. This implies involvement of one electron in the rate-limiting step of LeTID defect formation. The result not only is an important contribution to elucidate the physical mechanism underlying LeTID, but can also be used as a guideline for devising degradation tests of multicrystalline silicon wafers and solar cells.

1. Introduction

Light- and elevated temperature-induced degradation (LeTID) of multicrystalline silicon solar cell parameters and carrier lifetime has received significant attention due to its negative impact especially on highly efficient passivated emitter and rear contact (PERC) solar cells [1]. Besides illumination, the characteristic defect degradation can also be observed upon current injection, pointing towards a carrier-induced degradation (CID) mechanism [2]. Apart from that, the defect creation mechanisms as well as the participating components are still unclear: multicrystalline silicon wafers from different material suppliers differ in the degradation extent [2,3] and gettered wafers degrade less than ungettered sister samples [4], indicating that some impurity present in the starting material is involved. In addition, the degradation extent is strongly affected by solar cell processing steps: for example, a higher firing temperature peak leads to stronger degradation [3,5,6]. The temperature ramps are crucial for the degradation extent with fast temperature ramps (typical e.g. for fast firing ovens) causing stronger degradation, whereas slow temperature ramps decrease or even fully suppress LeTID, even for high peak temperatures [7]. A similar result can be obtained when adding a second fast-firing step featuring a lower peak temperature [6]. Also, the surface passivation layer has been shown to influence the degradation and regeneration behaviour [8].

The necessity of a high peak firing temperature for observation of LeTID has led to the hypothesis that the responsible impurity is initially present as precipitates, which need to be dissolved in order be able to act as LeTID "precursor" [5]. Either as an alternative or a complementing explanation to this hypothesis, the presence of hydrogen seems to be necessary for LeTID activation [8]. Either way the fact that the carrier lifetime degrades over an extended period of time suggests an interaction between two or more components, which undergo a transformation under degradation conditions. It is likely that this transformation is either related to the dissociation of an impurity complex (a prominent example for such a mechanism is the reaction $Fe^+B^- \rightarrow Fe_i^+ + B^-$ under illumination) or the formation of one. Please note that several authors already have ruled out the possibility that the known metastable defects Fe_i/FeB and boron-oxygen cause LeTID [1,2,9].

In addition to the degradation, it is observed that after a certain time, regeneration of the solar cell parameters / carrier lifetime occurs [2].

Degradation and regeneration kinetics strongly depend on the injection conditions and the temperature [2,10]. It is known that higher injection and/or higher temperature accelerate the degradation / regeneration cycle [2,10]. This can be exploited for very fast – and potentially industrially feasible – regeneration processes [10,11]. Recently, another significant influence has been identified: As *Chan et al.* showed, annealing LeTID-susceptible samples in the dark in the order of minutes to hours prior to illumination at elevated temperature alters the subsequent degradation and regeneration behaviour significantly

---

[12]. The underlying mechanisms appear to be nonlinear and are not yet understood: whereas dark annealing temperatures in the range of 125 °C to approx. 200 °C accelerate both degradation and regeneration compared to an untreated sample, a slightly higher temperature (~225 °C) first extremely slows down regeneration, followed by a slowed degradation and suppressed regeneration when going to even higher temperatures. *Chan et al.* noted that due to this dependence on the thermal history, studies investigating the degradation and regeneration kinetics might draw different conclusions due to even minute differences in thermal budget.

While keeping these findings in mind, studying the degradation and regeneration kinetics can provide insight into the physical processes during defect formation / annihilation. Such studies therefore are important for the identification of the root-cause defect and possibly assist in its mitigation without the necessity of complicating solar cell process adjustments.

However, the defect reaction rates as a function of carrier injection or temperature have not been quantified, yet. This work presents a study of the degradation rate constant in solar cells in dependence of the excess carrier density at the p-n junction $\Delta n(0)$ at constant temperature.

2. Approach

2.1. Samples

Full size 156 mm × 156 mm PERC solar cells were provided by an industrial manufacturer. They were processed from p-type high performance multicrystalline (HPM) silicon wafers from three different material suppliers. The materials were chosen to constitute a representative cross-section of standard commercially available wafers incorporating variations in impurity content, overall material quality and doping concentration. The three different materials are called "HPM1″ (base resistivity 1.7 Ω cm), "HPM2″ (2.2 Ω cm) and "HPM3″ (1.9 Ω cm) in the following.

Being aware of the influences of the solar cell process steps, the process parameters were chosen to enable maximum LeTID effect. All solar cells were processed in the same run without any process variations. As no additional post-anneal was performed [12], we expect the solar cells to show the "standard" degradation under injection at elevated temperature.

2.2. Experimental

The degradation conditions of most studies of the LeTID effect published so far applied constant illumination and thus a constant electron-hole generation rate. In this approach, the concentration of excess charge carriers Δn significantly decreases over time as a result of the carrier lifetime degradation. However, in order to determine the degradation rate constant R_{deg} as a function of Δn, the excess charge carrier density should remain as constant as possible.

In this study the solar cells were therefore degraded in the dark by applying a constant voltage over time. In this approach, the excess charge carrier density at the p-n junction $\Delta n(z=0)$ was kept constant according to

$$\Delta n(0) \approx \frac{n_i^2}{N_A} \exp\left(\frac{qV_a}{k_B T}\right),$$
(1)

with n_i the intrinsic carrier density, N_A the doping concentration, q the elementary charge, V_a the applied voltage, k_B the Boltzmann constant and T the temperature. Although the integrated carrier density still depends on bulk carrier lifetime to some degree, with this approach carrier density variation with time is minimal.

All samples were degraded at the same temperature of 75 °C ± 3 °C. During degradation, the current through the solar cell was
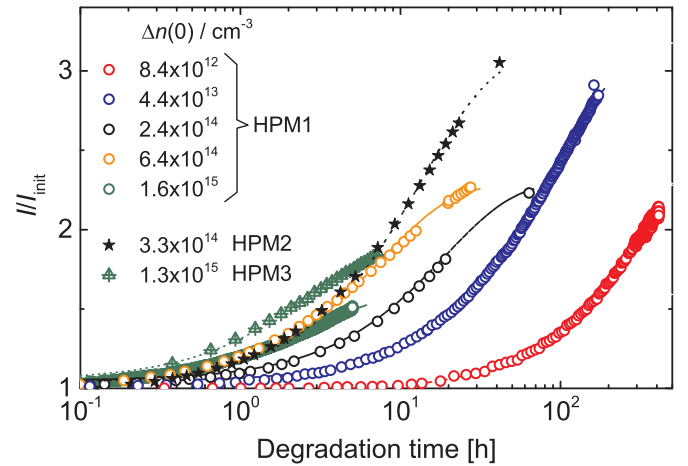

Fig. 1. Semi-logarithmic plot of the relative current increase versus degradation time. The degradation rate constant was obtained by fitting Eq. (2) to the data that is indicated by the dashed and dotted lines.

repeatedly measured. The observed increase can be entirely attributed to an increase of the saturation current density J_0, as the exponential term of the diode equation remains constant. Following *Cuevas'* interpretation of the "recombination parameter" J_0 [13], the change in saturation current density is proportional to the change in the defect density N_t.

In addition, electroluminescence images were taken at the same time steps as the current measurements for several samples degraded at different voltages. Thus, the temporal evolution of the excess carrier density averaged over the solar cell depth could be analyzed and compared to the determined value at the p-n junction.

3. Results

In Fig. 1, exemplary current measurements of several solar cells are plotted versus the degradation time. For better comparison, all values I are normalized to the respective initial current measurement I_{init}. It is obvious that with increasing $\Delta n(0)$ (corresponding to increasing applied voltage V_a) degradation proceeds faster. Please note that the degradation at the highest voltages (green symbols) was stopped when the current limit of the power supply was reached.

In most cases, the current increase over degradation time is well described by first-order reaction kinetics, which was used to obtain the degradation rate constants R_{deg} by fitting to the proportionality

$$\frac{I}{I_{init}} \propto (1-\exp(-R_{deg}t)).$$
(2)

Such fits are shown by the dashed and dotted lines in Fig. 1. Please note that it is not necessary to reach the saturation level in order to find a reliable value for R_{deg} provided that the degradation evolution has been tracked for a sufficiently long duration. On the other hand, by restricting the fit range to degradation times before saturation, the influence of the regeneration, which is believed to be a parallel process, on the current is expected to be minimal.

In a few cases the degradation behaviour showed indications of a two-stage progression with a fast and a slow component similar to the observation made by *Bredemeier et al.* [5] on lifetime samples. An example is shown in Fig. 2. Nevertheless, the exponential fit using Eq. (2) consistently yields reduced χ^2 values $< 10^{-2}$ for all experiments. In addition, when adding a second exponential to the fit function, both determined degradation rate constants $R_{deg,fast}$ and $R_{deg,slow}$ show the same general trends in dependence of $\Delta n(0)$ as R_{deg} from a Eq. (2) (an increased scatter occurred due to potential over-determination of the fits).

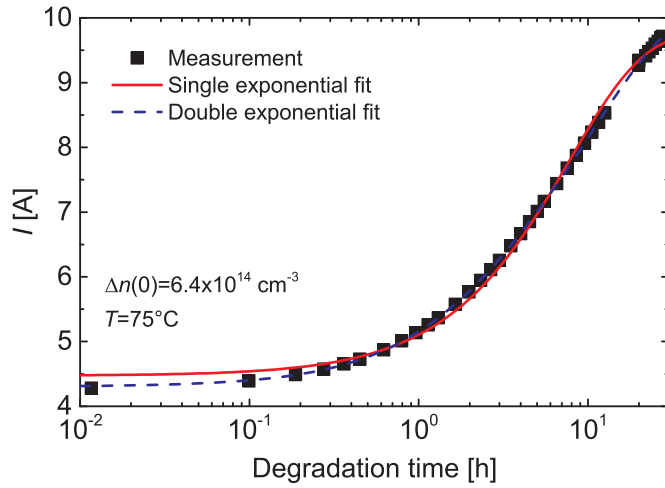In Fig. 3, the degradation rate constants fitted to measured curves of

Fig. 2. Relative current increase over degradation time, exemplarily showing indications for a two-stage progression with an initial fast component (up to approx. 1 h.) and a subsequent slow component. The fits using Eq. (2) (labelled "Single exponential fit") and the same equation but extended by a second exponential ("Double exponential fit") are shown by the continuous and dashed lines, respectively.
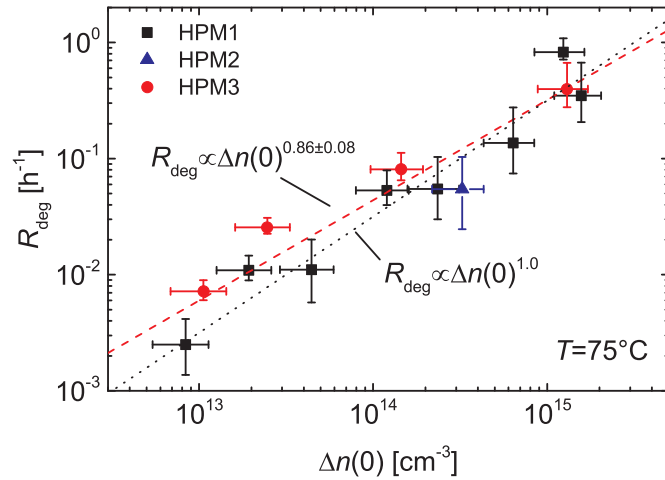

Fig. 3. Degradation rate constant plotted versus the excess carrier density at the p-n junction.

all investigated samples are plotted versus the respective excess electron concentration at the p-n junction $\Delta n(0)$. The error bars indicate the uncertainties calculated via error propagation (assumed uncertainty values: $\Delta N_A = 10\%$, $\Delta T = 3$ K, $\Delta V_a = 4$ mV). In addition, by analysing the electroluminescence images we notice a decrease in the excess carrier concentration Δn_{ave} averaged over the solar cell depth during the degradation. This decrease can amount to as much as 30% relative (compared to expected relative decrease of > 70% for the experimental case of constant illumination) in the investigated time range depending on the excitation conditions. We therefore systematically underestimate the degradation rate constant and the resulting error is also contained in Fig. 3, calculated by assuming a linear dependence of R_{deg} on Δn (see discussion below).

Although the degradation extent, *i.e.* the difference between the current values in the degraded and the initial state, differs for the different materials (indicated e.g. by the different saturation levels of HPM1 and HPM3 at $\Delta n(0)$ of 1.6 and 1.3×10^{15} cm^{-3}, respectively, green symbols in Fig. 1), similar degradation rate constants are obtained for comparable values of $\Delta n(0)$.

We observe a monotonous increase of R_{deg} with $\Delta n(0)$ in the entire excitation range investigated in this study. Specifically, no threshold or saturation level of the degradation rate constant is obvious. It is striking

that R_{deg} increases almost linearly with $\Delta n(0)$ (dashed line in Fig. 3), the best fit of the (scattered) data yielding a proportionality $R_{deg} \sim \Delta n(0)^{0.86 \pm 0.08}$, indicated by the dotted line.

4. Discussion

4.1. Rate limitation

No significant difference in the degradation rate constants R_{deg} between the different materials is observed for the equally processed samples under test.

The monotonicity of R_{deg} with $\Delta n(0)$ indicates that the supply of excess electrons determines the formation rate of the LeTID defects. What is more, the exponential being close to unity (dashed line in Fig. 3) suggests that the rate-limiting step of each defect activation/ formation involves one electron. The most likely explanation is that the initial compound or at least one of the participating components has to change its charge state as a prerequisite for the defect formation. In this picture, the degradation rate (the change of the concentration $[A](t)$ of LeTID "precursors" per time unit) is proportional to the absolute number of precursors occupied by an electron $[A]^-(t)$:

$$-\frac{d[A](t)}{dt} \propto [A]^-(t). \tag{3}$$

In a first order reaction, the term at the left equals the degradation rate constant multiplied by the concentration at time t. The right-hand side can be derived from the Shockley-Read-Hall (SRH) statistics to

$$[A]^-(t) = f_t [A](t). \tag{4}$$

with f_t denoting the relative fraction of LeTID precursors occupied by an electron, which will be discussed in detail further below. We re-write Eq. (3) to

$$R_{deg}[A](t) \propto f_t [A](t), \tag{5}$$

which shows the link between the degradation rate constant and the occupancy fraction. We assume here that (i) the relaxation time to equilibrium in the electron occupation is negligible compared to the rate-limiting step of the process, which is certainly fulfilled, and (ii) that the proportionality is constant over time. To illustrate the latter condition, for example one can think of the LeTID precursor consisting of two impurities, $X^+ Y$, bound via Coulombic attraction. If the positively charged impurity changes its charge state, both atoms become mobile relative to another as long as X is neutral, and if they separate, one or both of them represent the recombination-active LeTID defect. However, some atom pairs will stay close to each other and re-form the LeTID precursor as soon as X^0 loses an electron. Condition (ii) means that the relative fraction of LeTID precursors managing to separate from each other stays constant over time and for example does not depend on the concentration.

The relative fraction of precursors occupied by an electron f_t (or occupancy probability) is determined by the energy level E_t and the ratio of the capture cross sections for electrons and holes $k = \sigma_e/\sigma_h$ of the "precursor trap" and depends on temperature and excess carrier concentration. It can be written as [14].

$$f_t = \frac{1}{1 + \frac{kn_1 + p}{kn + p_1}}. \tag{6}$$

Here, n and p denote the total densities of electrons and holes (including excess charge carriers) in the conduction and the valence band, respectively, and n_1 and p_1 are the SRH densities of electrons and holes (and functions of E_t), respectively.

Using the proportionality in Eq. (5), the determined $R_{deg}(\Delta n(0))$ curve imposes some restrictions to possible E_t-k value pairs. An illustrating example is given in Fig. 4: For the case of $k = 28$ (a value which has been associated with the fully recombination-active LeTID defect
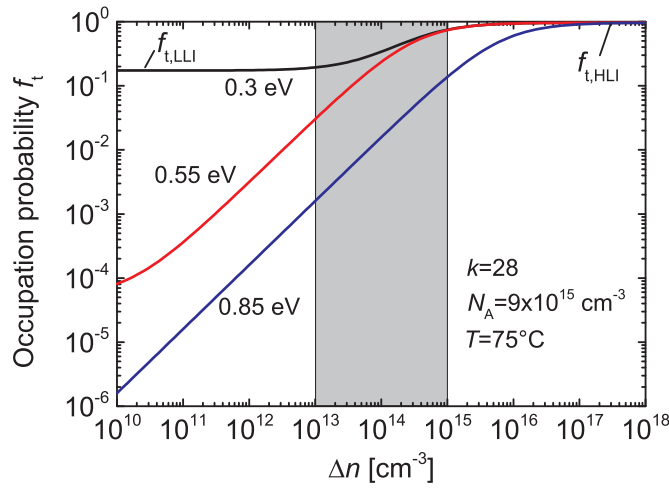
Fig. 4. Example for the occupancy probability f_t as a function of excess carrier density Δn for different energy levels E_t-E_V and an assumed capture coefficient ratio $k = 28$. Linearity in the region $\Delta n \sim 10^{13}$–10^{15} cm^{-3} (shaded area) is only observed for a certain E_t range.

level dominating the charge carrier lifetime [3,15]), the probability of an electron occupying a defect energy level near the valence band edge E_V (black line, E_t-E_V = 0.3 eV) is very high even at very low excess carrier densities. Hence, for the value pair 0.3 eV and k = 28 we would expect a shape of $R_{\text{deg}}(\Delta n(0))$ with an exponent significantly below 1. With an assumed energy level at midgap (red line, E_t-E_V = 0.55 eV), the occupancy probability begins to saturate at excess carrier densities above 10^{14} cm^{-3}, which leads to the expectation that the shape of the $R_{\text{deg}}(\Delta n(0))$ curve should deviate from linearity towards higher injection. On the other hand, for energy levels in the upper bandgap half (e.g. blue line, E_t-E_V = 0.85 eV), the occupancy probability f_t and thus $R_{\text{deg}}(\Delta n(0))$ increases linearly with the excess carrier density in the Δn-range of interest.

Following from Fig. 3, we search for value pairs of E_t and k that lead to an approximately linear increase in f_t of more than two orders in magnitude in the Δn range $\sim 10^{13}$–10^{15} cm^{-3}. The following general considerations assume p-type Si base material, but can be extended to any semiconductor material.

In high level injection (HLI), where $n \gg N_A$, n_1 and p_1,

$$f_{t,HLI} \to \frac{1}{1+\frac{1}{k}}. \tag{7}$$

In low level injection (LLI), where p approximately equals N_A,

$$f_{t,LLI} \to \frac{1}{1+\frac{N_A}{p_1}}. \tag{8}$$

Examples for these limits are marked in Fig. 4. In the intermediate range between low and high level injection, f_t approximately follows a linear relationship in Δn as long the difference between $f_{t,LLI}$ and $f_{t,HLI}$ is large enough. In order to have a dynamic range of f_t values of a factor x for example

$$f_{t,HLI} > x f_{t,LLI}, \tag{9}$$

we find the restriction

$$E_t - E_V > -k_B T \ln\left[\frac{N_A}{N_V\left(x\left(1+\frac{1}{k}\right)-1\right)}\right]. \tag{10}$$

Here, N_V denotes the effective density of states in the valence band, k_B is the Boltzmann constant and T the temperature.

Let $x \gg 1$, we find for the extreme cases of $k \ll 1$:

$$E_t - E_V > -k_B T \ln\left[\frac{N_A}{N_V x k^{-1}}\right], \tag{11}$$

and for $k \gg 1$:

$$E_t - E_V > -k_B T \ln\left[\frac{N_A}{N_V x}\right]. \tag{12}$$

The latter also represents the minimum value for E_t.

This first consideration to narrow down the range of possible E_t-k pairs is based on the observed increase in f_t. A further restriction of possible E_t-k pairs comes from the range of Δn values in which the linear increase was observed (shaded area in Fig. 4). In fact, f_t in high level injection saturates at excess carrier densities mostly determined by the ratio

$$\frac{kn}{kn_1+p}. \tag{13}$$

Let Δn_{HLI} be the upper boundary of the linear range, then linearity is determined by Eq. (10) alone as long as

$$k \leq \frac{p}{\Delta n_{HLI}} \approx \frac{N_A}{\Delta n_{HLI}}. \tag{14}$$

For larger k values, saturation sets in at lower excess carrier densities. Therefore, linearity is only ensured for the same upper boundary Δn_{HLI} if the SRH density n_1 comes into play in Eq. (13). This relation is illustrated in Fig. 4 by the two curves with E_t - E_V = 0.55 eV and 0.85 eV. We find the second restriction

$$E_t - E_V > k_B T \ln\left[\frac{\Delta n_{HLI} - \frac{p}{k}}{N_C}\right] + E_G \approx k_B T \ln\left[\frac{\Delta n_{HLI} - \frac{N_A}{k}}{N_C}\right] + E_G. \tag{15}$$

N_C denotes the effective density of states at the conduction band edge and E_G is the bandgap width. For $k \gg 1$, Eq. (15) approaches the constant value

$$E_t - E_V > k_B T \ln\left[\frac{\Delta n|_{HLI}}{N_C}\right] + E_G. \tag{16}$$

In Fig. 5, following from Eqs. (10) and (15) an estimate for possible E_t-k value pairs is displayed for material "HPM1" and our results for the degradation rate constant R_{deg}. All necessary parameterizations with regard to T were taken from reference [16]. It can be seen that the defect level triggering the degradation has to be at least ~ 0.4 eV above the valence band edge, independent of its capture cross section ratio. If k is larger than ~ 50, E_t has to be relatively close to the conduction band edge. For $k < 1$, E_t slowly increases following Eq. (11).
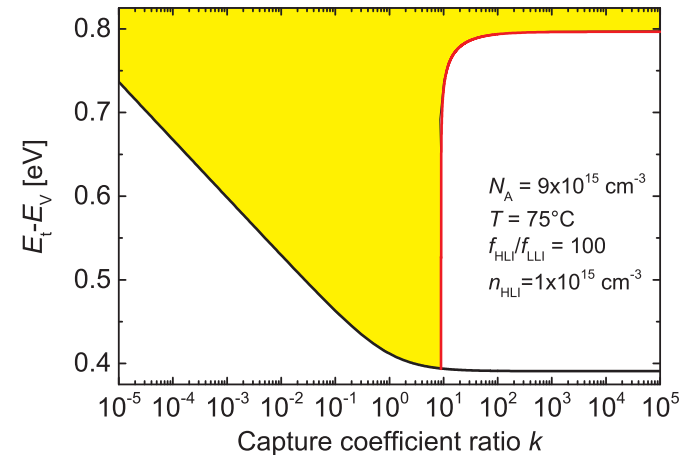

Fig. 5. Possible E_t-k value pairs (yellow area) for which a linear increase of f_t of about two orders of magnitude is expected in the range up to $\Delta n = 10^{15}$ cm^{-3}, using Eq. (10) (black continuous line) and Eq. (15) (red).

To summarize, if the assumptions that (i) degradation is triggered by the change of charge states of a defect in the wafer bulk and (ii) the degradation rate is limited by the occupancy probability of this state are valid, a reasonable estimate for the underlying SRH defect properties can be derived as discussed above and as illustrated in Fig. 5. Taking the relatively high measurement uncertainties and the limited investigated injection range into account, it seems possible yet unlikely that a defect level with $k \approx 28$ (which appears to dominate recombination activity introduced by LeTID in degraded state [3,15]) is also responsible for the initial defect emergence (see also Fig. 4). If it is, then the energy level probably lies in the upper half of the bandgap. The same holds true for the recent parameterizations by *Vargas et al.,* who suggested possible energy levels of E_t - E_V = (0.24 ± 0.05) eV with a capture coefficient ratio k of (56 ± 23) or E_t - E_V = (0.77 ± 0.05) eV with k = (49 ± 21), respectively [17]. We can definitely rule out the possibility that the energy level positioned in the lower band gap half triggers the degradation. The suggested level in the upper band gap half seems possible yet unlikely.

In principle, the defect determining the degradation reaction kinetics should also introduce recombination activity and thus impact charge carrier lifetime prior to degradation. Since we do not know the defect concentration and the capture cross sections, its expected influence on carrier lifetime cannot be quantified at this stage. The observation of relatively high lifetimes exceeding 100 μs even at low level injection (see e.g. Fig. 3 in reference [2]) does not stand in contradiction with our estimates of possible E_t-k value pairs.

This study focuses on carrier-induced degradation and therefore no insights into the regeneration mechanism were derived from experiments. However, it should be noted that our proposed model describing the degradation mechanism can be extended by a likely explanation for the regeneration: once the LeTID precursor complex splits into independently mobile species X and Y, these could diffuse to sinks like crystal defects or the wafer surface, resulting in decreasing recombination activity. This mechanism would be in agreement with suggestions in literature, e.g. by Bredemeier et al. [5].

4.2. Implications for degradation studies

The strong injection dependence of the degradation rate needs to be considered when investigating the degradation kinetics of lifetime samples in particular. In contrast to our study where the external bias keeps the excess electron concentration fixed (at least at the p-n junction), studies based on constant illumination of lifetime samples might suffer from a drop in Δn_{ave} by a factor of four and more within a short time [5,6]. As a result, the degradation rate drops by almost the same factor as degradation proceeds, which should be kept in mind when analysing the degradation kinetics of lifetime samples.

In principle, a fast and convenient way to assess and compare LeTID of different solar cells is to measure the relative change of solar cell parameters during a fixed time of for example 24 h at 1000 W/m^2 illumination at 75 °C [2]. This procedure mainly reflects the impact of the open circuit voltage on the degradation rate. Depending on the aim of the investigation, a better comparability may often be achieved by applying the same voltage in the dark to the different solar cells.

5. Conclusion

In this study, the degradation rate constant of carrier-induced degradation at elevated temperature was shown to depend (almost) linearly on the excess charge carrier density in high performance multicrystalline silicon PERC solar cells, independent of the base material. A possible explanation of this finding is that the LeTID precursor has to change its charge state as a pre-condition for degradation. By linking

the degradation rate constant with the occupation probability of a defect in the bandgap described by SRH statistics, we are able to narrow down the range of possible SRH parameters of the LeTID precursor defect level.

Extended application of the demonstrated approach could provide further limitations on the SRH parameters, which could eventually lead to the identification of the responsible precursor defect. To this end, a wide range of excess carrier densities should be investigated aimed at identifying the characteristic threshold and saturation values of the degradation rate constant predicted by SRH statistics. If necessary, these investigations may be accompanied by variations of the doping concentration and/or the temperature. However, it must be kept in mind that these variations also influence other mechanisms, in particular the regeneration, which is thought to run in parallel to degradation.

References

[1] K. Ramspeck, S. Zimmermann, H. Nagel, A. Metz, Y. Gassenbauer, B. Birkmann, A. Seidl, Light Induced Degradation of Rear Passivated mc-Si Solar Cells, in: 27th EUPVSEC Frankfurt: 2012, Frankfurt, 2012, pp. 861–865.

[2] F. Kersten, P. Engelhart, H.-C. Ploigt, A. Stekolnikov, T. Lindner, F. Stenzel, M. Bartzsch, A. Szpeth, K. Petter, J. Heitmann, J.W. Müller, Degradation of multicrystalline silicon solar cells and modules after illumination at elevated temperature, Sol. Energy Mater. Sol. Cells 142 (2015) 83–86.

[3] K. Nakayashiki, J. Hofstetter, A.E. Morishige, T.-T.A. Li, D.B. Needleman, M.A. Jensen, T. Buonassisi, Engineering solutions and root-cause analysis for light-induced degradation in p-type multicrystalline silicon PERC modules, IEEE J. Photovolt. 6 (4) (2016) 860–868.

[4] A. Zuschlag, D. Skorka, G. Hahn, Degradation and regeneration in mc-Si after different gettering steps, Prog. Photovolt.: Res. Appl. (2016).

[5] D. Bredemeier, D. Walter, S. Herlufsen, J. Schmidt, Lifetime degradation and regeneration in multicrystalline silicon under illumination at elevated temperature, AIP Adv. 6 (3) (2016) 35119.

[6] C.E. Chan, D.N.R. Payne, B.J. Hallam, M.D. Abbott, T.H. Fung, A.M. Wenham, B.S. Tjahjono, S.R. Wenham, Rapid stabilization of high-performance multicrystalline P-type silicon PERC cells, IEEE J. Photovolt. 6 (6) (2016) 1473–1479.

[7] R. Eberle, W. Kwapil, F. Schindler, M.C. Schubert, S.W. Glunz, Impact of the firing temperature profile on light induced degradation of multicrystalline silicon, Phys. Status Solidi RRL – Rapid Res. Lett. 10 (12) (2016) 861–865.

[8] F. Kersten, J. Heitmann, J.W. Müller, Influence of Al$_2$O$_3$ and SiNx passivation layers on LeTID, Energy Procedia 92 (2016) 828–832.

[9] F. Fertig, K. Krauß, S. Rein, Light-induced degradation of PECVD aluminium oxide passivated silicon solar cells, Phys. Status Solidi RRL – Rapid Res. Lett. 9 (1) (2015) 41–46.

[10] D.N. Payne, C.E. Chan, B.J. Hallam, B. Hoex, M.D. Abbott, S.R. Wenham, D.M. Bagnall, Rapid passivation of carrier-induced defects in p-type multi-crystalline silicon, Sol. Energy Mater. Sol. Cells 158 (2016) 102–106.

[11] K. Krauß, A.A. Brand, F. Fertig, S. Rein, J. Nekarda, Fast regeneration processes to avoid light-induced degradation in multicrystalline silicon solar cells, IEEE J. Photovolt. 6 (6) (2016) 1427–1431.

[12] C. Chan, T.H. Fung, M. Abbott, D. Payne, A. Wenham, B. Hallam, R. Chen, S. Wenham, Modulation of carrier-induced defect kinetics in multi-crystalline silicon PERC cells through dark annealing, Sol. RRL 1 (2) (2017) 1600028.

[13] A. Cuevas, The recombination parameter J0, Energy Procedia 55 (2014) 53–62.

[14] C. Sun, F.E. Rougieux, D. Macdonald, A unified approach to modelling the charge state of monatomic hydrogen and other defects in crystalline silicon, J. Appl. Phys. 117 (4) (2015) 45702.

[15] A.E. Morishige, M.A. Jensen, D.B. Needleman, K. Nakayashiki, J. Hofstetter, T.-T.A. Li, T. Buonassisi, Lifetime spectroscopy investigation of light-induced degradation in p-type multicrystalline silicon PERC, IEEE J. Photovolt. 6 (6) (2016) 1466–1472.

[16] S. Rein, Lifetime Spectroscopy: A Method of Defect Characterization in Silicon for Photovoltaic Applications, 1st ed., Springer, Berlin, New York, 2005.

[17] C. Vargas, Y. Zhu, G. Coletti, C. Chan, D. Payne, M.A. Jensen, Z. Hameiri, Recombination parameters of lifetime-limiting carrier-induced defects in multicrystalline silicon for solar cells, Appl. Phys. Lett. 110 (9) (2017) 92106.